Extensive liquid meltwater storage in firn within the Greenland ice sheet 1 2 **Authors:** Richard R. Forster<sup>1\*</sup>, Jason E. Box<sup>2,3</sup>, Michiel R. van den Broeke<sup>4</sup>, Clément Miège<sup>1</sup>, Evan W. 3 Burgess<sup>1</sup>, Jan H. van Angelen<sup>4</sup>, Jan T. M. Lenaerts<sup>4</sup>, Lora S. Koenig<sup>5</sup>, John Paden<sup>6</sup>, Cameron 4 Lewis<sup>6</sup>, S. Prasad Gogineni<sup>6</sup>, Carl Leuschen<sup>6</sup>, Joseph R. McConnell<sup>7</sup> 5 6 7 **Affiliations:** <sup>1</sup>Department of Geography, University of Utah, Salt Lake City, UT, USA 8 9 <sup>2</sup>Geological Survey of Denmark and Greenland (GEUS), Copenhagen, Denmark <sup>3</sup>Byrd Polar Research Center, The Ohio State University, Columbus, OH, USA 10 <sup>4</sup>Institute for Marine and Atmospheric Research Utrecht, Utrecht University, Utrecht, The 11 Netherlands 12 <sup>5</sup>NASA Goddard Space Flight Center, Greenbelt, MD, USA 13 <sup>6</sup>Center for Remote Sensing of the Ice Sheets, University of Kansas, Lawrence KS, USA 14 <sup>7</sup>Desert Research Institute, University of Nevada, Reno, NV, USA 15 \*Correspondence to: rick.forster@geog.utah.edu 16 17 The accelerating loss of mass from the Greenland ice sheet is a major contribution to current 18 19 sea level rise<sup>1</sup>. Increased meltwater runoff is responsible for half of Greenland's mass loss 20 increase<sup>2</sup>. Surface melt has been increasing in extent and intensity, setting a record for surface area melt and runoff in 2012<sup>3</sup>. The mechanisms and timescales involved in allowing surface 21 meltwater to reach the ocean where it can contribute to sea level rise are poorly understood. The 22 potential capacity to store this water in liquid or frozen form in the firn (multi-year snow layer) is 23 significant<sup>4</sup>, and could delay its sea-level contribution. Here we describe direct observation of 24 water within a perennial firn aquifer persisting throughout the winter in the southern ice sheet, 25 where snow accumulation and melt rates are high. This represents a previously unknown storage 26 mode for water within the ice sheet. Ice cores, ground/airborne radar and a regional climate 27 model are used to estimate aguifer area  $(70 \pm 10 \times 10^3 \text{ km}^2)$  and water table depth (5-50 m). The 28

perennial firn aquifer represents a new glacier facies to be considered in future ice sheet mass and energy budget calculations.

29

30

31

32

33

34

35

36

37

38

39

40

41

42

43

44

45

46

47

48

49

50

51

The mass of liquid or refrozen meltwater that could be stored in firn pore space throughout the percolation zone of the entire ice sheet is estimated to be between 322 and 1,289 Gt<sup>4</sup>. In the western part of the ice sheet, the possibility of liquid water persisting within the upper ~10 m of the snow/firn<sup>5</sup> or in moulins<sup>6</sup> during winter is suspected. Discharge measurements at ice marginal streams indicate winter water release, suggesting that some meltwater may be stored englacially or at the bed and is released months after the end of the melt season<sup>7</sup>. However, there has been no account of directly observed liquid water in the firn persisting through the winter on the Greenland ice sheet. In April 2011, prior to seasonal surface melt onset, the Arctic Circle Traverse (ACT) expedition drilled into a liquid water layer in the upper 10 to 25 m of the firn in southeast Greenland. The ACT field party extracted four firn cores at sequentially lower elevations on the southeast coast (Fig. 1), where in situ snow accumulation observations were previously nonexistent. Below 1600 m in this area, spatially and temporally averaged accumulation rates of 1-4 m w.e. a<sup>-1</sup> are simulated by observationally-constrained regional climate models<sup>8, 9, 10</sup>. On 30 April 2011, at ACT11-A2 (1559 m a.s.l.), a 10 cm diameter firn/ice coring drill extracted a ~1 m core segment from 10 m depth that was saturated with liquid water (Fig. 1). The following day, 3 km to the east at ACT11-A (1589 m a.s.l.), liquid water was found at 25 m depth using the drill. The thickness of the water layer could not be measured because the drill is not designed to operate in water. Air temperatures were -15 °C during drilling. During spring 2011, temperatures

Therefore, the liquid water found in the firn no doubt persisted throughout the winter. The other

were below average and surface melt in the area did not commence until June that year<sup>11</sup>.

two ACT cores were extracted at higher elevations nearby (1806 and 2081 m a.s.l.) and revealed no liquid water to the full depth of the 61 m drilling (Fig. 1).

Ground penetrating radar (GPR, Supplementary Information) profiles were completed between the core sites, as well as 10 km below the lowest site. A strong contiguous return horizon persists over the lower 25 km portion of the transect (Fig 2). The horizon undulates between depths of 9-25 m and matches the depth of the water layer top found at both core sites to within < 1 m (the precision of identifying the depth is limited to the 1 m length core sections drilled). We are thus confident that the GPR is tracing the top of the water layer.

The top of the water layer cuts across intermediate GPR horizons (Fig. 2), usually interpreted as corresponding with annual or event accumulation layers<sup>12, 13</sup>. Below the water layer horizon there are no coherent GPR horizons, which can be expected as minimal energy is returned from below a strong reflector with a high permittivity contrast such as water<sup>14</sup>. The bright horizon gradually fades at the 25 km location at a depth of ~27 m (Fig. 2), revealing internal firn layers to depths of ~50 m that are traceable up-glacier over the next 82 km to cores ACT11-B and C (Fig. 1).

The NASA Operation Ice Bridge (OIB) airborne accumulation radar (AR)  $^{15}$  overflew the core sites and the ground traverse GPR transect 11 days prior to the core drilling. A strong reflecting horizon is evident at the same location in the GPR transect [Supplementary Fig. S1]. The depth to the bright horizon from the GPR and AR agree within 2 m over the 25 km transect and the undulations are very similar [ $r^2 = 0.95$ , Supplementary Fig. S2]. The depth differences may be attributed to lateral discrepancies in the transect locations (< 200 m), and differences in radar foot print size and radar frequency. Similar to the GPR data, the AR returns no obvious internal layering below the bright horizon [Supplementary Fig. S1]. Based on the depth

agreement and high correlation we conclude that the AR is capable of mapping the presence and depth to the top of the water layer within the firn.

In 2011, prior to melt onset, NASA OIB AR gathered 40,512 km of horizontal flight line data over the GrIS (March 29 — May 16). All of these flight lines were examined for the presence of the water layer. It was identified and manually digitized in 843 km of these flight lines acquired between April 8-26, 2011 (Fig. 1). The water layer locations are concentrated in the southeast, but are evident in isolated locations in the south and southwest and on the Geikie Plateau (near 70° N, 25° W). The mean depth of the water layer top is 23 m with a range of 5 to 50 m [Supplementary Figs. S3 and S6]. In general the depths are smaller in the southwest compared to the southeast, but are influenced by local surface slope (Fig. 2), similar to terrestrial groundwater and firn aquifers on temperate glaciers <sup>16, 17</sup>. Thus, we refer to this liquid water reservoir that persists throughout the winter as a perennial firn aquifer (PFA). Since the radar signal is not returning from below the top of the PFA, there is currently no direct measure of its thickness.

The spatial distribution of the PFA suggests that its formation is associated with areas of sufficient surface melt coupled with high accumulation. We compare the PFA extent as determined by AR results with gridded climate fields. Here we use the accumulation field from the Calibrated Polar MM5<sup>10</sup> (Fig. 3) and output fields of accumulation, melt and rain from the regional atmospheric climate model RACMO2 [Supplementary Fig. S5]. RACMO2 includes an interactive (with the atmosphere) snow/firn/ice model<sup>8</sup>. In areas where the PFA is found, the mean accumulation rate is 1.24/2.22 m w. e. a<sup>-1</sup> (10 and RACMO2, respectively). However, there is significant variability in the range of accumulation rate associated with the PFA [Supplementary Fig. S6]. (Supplementary Information for discussion of the differences in these

accumulation grids) Areas of high accumulation are found predominately in the southeast, but three other areas in the south and southwest are also identified with local accumulation maxima and also contain a PFA (Fig. 3).

The spatial pattern of the PFA extent for April 2011 simulated by RACMO2 is very similar to the AR results, with a concentration in the southeast and the three areas in the south and southwest (Fig. 4). In RACMO2, a combination of high accumulation (> 800 mm yr<sup>-1</sup>) and a large liquid water production (snow melt plus rain > 650 mm yr<sup>-1</sup>) are necessary conditions for PFA formation [Supplementary Fig. S7]. Because RACMO2 performs well in detecting the PFA, we use it as a first order estimate of PFA spatial extent. Since the model lacks treatment of potentially significant firn processes, i.e. inhomogeneous vertical water flow (piping) which moves water to depth through cold snow/firn<sup>5, 18, 19</sup> and horizontal water flow, which as Fig. 2 shows is an important process, an estimate of PFA volume is not given here. For uncertainty in the modeled PFA extent we use the variability in annual minimum extents during 1992-2011, which are typically reached in late April at  $70 \pm 10 \times 10^3 \text{ km}^2$ , [Supplementary Fig. S8]. After the onset of the melt season, extent of liquid water in the Greenland firn sharply increases, to reach  $500 \pm 250 \times 10^3 \text{ km}^2$  in July, after which a gradual decrease is simulated.

The formation process of the PFA is not completely understood; however, its spatial correspondence with high accumulation and melt rates (Fig. 3, Supplementary Fig. S7) leads to a general hypothesis intended to explain the broad pattern of PFA location. From the RACMO2 model results, we propose that high accumulation insulates the melt season's liquid water layer within the firn from the cold season atmosphere, thereby preventing complete refreezing. This allows liquid water to persist throughout the winter until the next melt season, when the PFA may be recharged [movie S1].

The PFA represents a new glacier facies 18 and a previously unidentified liquid water reservoir. Its location in the southeastern ice sheet is consistent with few surface lakes, compared to other sectors of the ice sheet<sup>20</sup>. The narrow (< 30 km) ablation area with minimal bare ice area in the southeast, due to the relatively high accumulation gradients and therefore steep ice slopes, does not accommodate lake basin formation with accompanying supra glacial stream networks and moulins delivering water toward the bed as prevalent along the western portion of the ice sheet. In its place, the deep firn layer provides an alternative liquid water reservoir in winter, which may exceed the mass of liquid water stored in supraglacial lakes. This contrast in liquid water storage mechanisms implies that surface mass balance, thermal properties of the ice, and effective water pressures at the bed and consequently ice dynamics in the southeast are likely very different from those in the more extensively studied western and northern Greenland ice sheet. The persistence of liquid water in the firn also has implications for the ice sheet energy. If atmospheric warming ceases, refreezing the liquid water requires a significant amount of additional energy before the firn layer can start to cool. The PFA could thus represent an increasingly important mass and energy reservoir, as both melt and accumulation on the Greenland ice sheet have increased in the past<sup>21</sup> and are projected to increase in a future warming climate<sup>22</sup>.

138

139

140

141

142

143

121

122

123

124

125

126

127

128

129

130

131

132

133

134

135

136

137

## Methods

GPR data were collected with a Geophysical Survey Systems, Inc. SIR-3000 controller and a 400 MHz center frequency antenna. The vertical resolution in firn is 35 cm<sup>12, 13</sup>, finer than the annual layering in this area. The sampling was set at four traces per second, 2048 samples per trace. To increase the signal-to-noise ratio an initial stacking of six traces was performed. Post

processing horizontal spatial smoothing involved averaging an additional eight traces, to increase the signal-to-noise ratio and minimize the influence of cm-scale vertical ice pipes or channels present in the percolation zone<sup>13</sup>. A time dependent gain was used to compensate for signal attenuation within the firn. The maximum two-way-travel time (TWT) range was set to 500 ns, yielding a ~0.24 ns sample interval and allowing scanning of the top ~46 m of the firn. Because the top of the water layer is mostly found in the upper firn column, radar TWT is converted to depth below the surface assuming a constant electromagnetic wave travel at 1.94x10<sup>8</sup> m s<sup>-1</sup> into the firn. This travel velocity corresponds to a depth-averaged firn density of 650 kg m<sup>-3</sup>. We compare this method with the TWT-depth conversion described by (13) using the relationship between velocity in the firn and ACT11-A firn density profile<sup>24</sup>. The difference between the two methods does not exceed 50 cm for the first 20 m of the firn column, and with the lack of detailed density profiles (despite at our firn-core locations), we favored the first method in our analysis.

The GPR did not have an integrated GPS, therefore a roving GPS unit was attached to the

The GPR did not have an integrated GPS, therefore a roving GPS unit was attached to the snowmobile towing the GPR sled and collected a point every five seconds.. GPS data processing was done using the on-line Canadian Spatial Reference Service - Precise Point Positioning. This processor uses GPS orbit and clock information to enhanced positioning precisions in the International Terrestrial Reference Frame via a kinematic processing mode. To geo-reference the final GPR radar data, the processed GPS data were used by matching the GPS time to the starting point of each GPR radar image in post processing to yield a 10 cm-scale topographic profile coincident with all GPR lines. A linear interpolation of the 5 s GPS points was made to obtain a GPS coordinates for each GPR trace.

The Accumulation Radar<sup>15</sup> (AR) is a combined stepped-chirped system built by the Center for Remote Sensing of the Ice Sheets (CReSIS), operates from 550 to 900 MHz when flown on a P3 aircraft typically 500 m above surface with a vertical resolution in ice of 28 cm over an effective footprint of approximately 30 m (https://www.cresis.ku.edu/). All of the AR radar images (example: fig. S1) from the NASA Operation IceBridge (OIB) flightlines were manually inspected for presence of a water layer representing the top of the PFA. This was characterized by a strong subsurface horizon with no internal layers below. The top of the PFA along with the snow surface was screen-digitized on the corresponding radar images. The time difference between the surface and reflection horizon was converted to depth to the top of the PFA using the same wave velocity of 1.94x10<sup>8</sup> m s<sup>-1</sup> as was used for the GPR depth calculations. A direct comparison between the depth to top of PFA derived from the GPR and AR is made for the 25 km segment centered on the cores that drilled to water (ACT-11A and ACT-11A2, fig. S2). The depth to top of the PFA along the OIB flight lines is shown in fig. S3.

While the spatial patterns between the PFA as mapped by the AR and simulated by

While the spatial patterns between the PFA as mapped by the AR and simulated by RACMO2 are similar (Fig. 4), potential reasons for their differences (apart from the obvious uncertainty in the model results) are described here. The areas of RACMO2 simulated PFA that are not mapped as PFA in AR flight lines may be due to several reasons: 1) water is present but subsurface returns from the radar are not detectable because strong surface returns (clutter) from rough crevassed surfaces mask the weaker water layer return, 2) water is present but subsurface returns from the radar are not detectable due to subsurface clutter (refrozen ice bodies above the water layer), 3) liquid water is not present due to internal drainage through crevasses, a process not included in RACMO2. Locations where surface crevassing is observed coincident with simulated RACMO2 PFA that is not detected by AR are shown in Fig. S4. These three scenarios

could explain the lack of mapped water layer along flight lines with modeled water over the lower elevation portions of the numerous outlet glaciers along the south east coast. The contrary situation, with mapped PFA that is not simulated, is isolated to areas in south west and could be associated with model uncertainty and limited model resolution.

## 194 **REFERENCES**

- 195 1. Rignot, E., Velicogna, I., van den Broeke, M. R., Monaghan, A. & Lenaerts, J. T. M.
- Acceleration of the contribution of the Greenland and Antarctic ice sheets to sea level rise.
- 197 Geophysical Research Letters 38, (2011).
- 198 2. van den Broeke, M. et al. Partitioning Recent Greenland Mass Loss. Science 326, 984–986
- 199 (2009).
- 3. Nghiem, S. V. et al. The extreme melt across the Greenland ice sheet in 2012. Geophysical
- 201 *Research Letters* **39**, (2012).
- 4. Harper, J., Humphrey, N., Pfeffer, W. T., Brown, J. & Fettweis, X. Greenland ice-sheet
- 203 contribution to sea-level rise buffered by meltwater storage in firn. *Nature* **491**, 240–243 (2012).
- 5. Humphrey, N. F., Harper, J. T. & Pfeffer, W. T. Thermal tracking of meltwater retention in
- Greenland's accumulation area. *Journal of Geophysical Research: Earth Surface* 117, (2012).
- 6. Catania, G. A. & Neumann, T. A. Persistent englacial drainage features in the Greenland Ice
- 207 Sheet. *Geophysical Research Letters* **37**, (2010).
- 7. Rennermalm, A. K., L. C. Smith, V. W. Chu, R. R. Forster, J. E. Box, and B. Hagedorn
- 209 Proglacial river stage, discharge, and temperature datasets from the Akuliarusiarsuup Kuua River
- 210 northern tributary, Southwest Greenland, 2008–2011. Earth System Science Data 4, 1–12 (2012).
- 8. van Angelen, J. H. *et al.* Sensitivity of Greenland Ice Sheet surface mass balance to surface
- albedo parameterization: a study with a regional climate model. The Cryosphere 6, 1175–1186
- 213 (2012).
- 9. Ettema, J. et al. Higher surface mass balance of the Greenland ice sheet revealed by high-
- resolution climate modeling. *Geophysical Research Letters* **36**, (2009).

- 216 10. Burgess, E. W. et al. A spatially calibrated model of annual accumulation rate on the
- Greenland Ice Sheet (1958–2007). *Journal of Geophysical Research: Earth Surface* **115**, (2010).
- 11. Tedesco M., J. E. Box, J. Cappellen, T. Mote, R. S. W. van de Wal, and J. Wahr Greenland
- 219 ice sheet: The state of the climate in 2011. *Bull. Amer. Meteor. Soc.* **93**, 148–151 (2012).
- 12. Arcone, S. A., Spikes, V. B., Hamilton, G. S. & Mayewski, P. A. Stratigraphic continuity in
- 400 MHz short-pulse radar profiles of firn in West Antarctica. *Annals of Glaciology* **39**, 195–200
- 222 (2004).
- 223 13. Miège, C. et al. Southeast Greenland high accumulation rates derived from firn cores and
- ground-penetrating radar. *Annals of Glaciology* **54**, 322–332 (2013).
- 225 14. Bogorodsky, V. V., Bentley, C. R. & Gudmandsen, P. E. Radioglaciology. (D. Reidel
- Publishing Company, Dordrecht, Netherlands: 1985).
- 15. Leuschen, C. IceBridge Accumulation Radar L1B Geolocated Radar Echo Strength Profiles.
- 228 April-May 2011. Boulder, Colorado USA: NASA DAAC at the National Snow and Ice Data
- 229 *Center* (2011).
- 230 16. Fountain, A. G. The storage of water in, and hydraulic characteristics of, the firn of South
- 231 Cascade Glacier, Washington State, U.S.A. *Annals of Glaciology* **13**, 69–75 (1988).
- 232 17. Fountain, A. G. & Walder, J. S. Water flow through temperate glaciers. *Reviews of*
- 233 Geophysics **36**, 299–328 (1998).
- 18. Benson, C. S. Stratigraphic studies in the snow and firn of the Greenland Ice Sheet. U.S.
- 235 Snow, Ice and Permafrost Research Establishment. 70, (U.S. Snow, Ice and Permafrost Research
- 236 Establishment Research Rep: 1962).
- 19. Pfeffer, W. T., Illangasekare, T. H. & Meier, M. F. Analysis and modeling of melt-water
- refreezing in dry snow. *Journal of Glaciology* **36**, 238–246 (1990).

239 20. Selmes, N., Murray, T. & James, T. D. Fast draining lakes on the Greenland Ice Sheet. 240 *Geophysical Research Letters* **38**, (2011). 241 21. Box, J. E. Greenland ice sheet mass balance reconstruction. Part II: surface mass balance 242 (1840-2010). Journal of Climate (2013).doi:http://dx.doi.org/10.1175/JCLI-D-12-00518.1 243 22. Fettweis, X. et al. Brief communication 'Important role of the mid-tropospheric atmospheric 244 circulation in the recent surface melt increase over the Greenland ice sheet'. The Cryosphere 7, 245 241-248 (2013). 246 23. Bamber, J. L., Ekholm, S. & Krabill, W. B. A new, high-resolution digital elevation model of 247 Greenland fully validated with airborne laser altimeter data. J. Geophys. Res. 106, PP. 6733– 248 6745 (2001). 249 250 251 **Supplementary Information** is available in the online version of the paper. 252 **Acknowledgments** This work was supported by National Science Foundation Office of Polar 253 Programs Award ARC-0909499, ARC-0909469, and the Polar Program of the Netherlands 254 Organization for Scientific Research (NWO/ALW). We acknowledge the use of data and/or data 255 products from CReSIS generated with support from NSF grant ANT-0424589 and NASA grant 256 NNX10AT68G. CH2MHill Polar Field Services provided vital logistical support. The NASA 257 airborne radar data can be obtained free of charge from the National Snow and Ice Data Center 258 (IceBridge Accumulation Radar L1B Geolocated Radar Echo Strength Profiles, April-May 259 2010).

260

261 Author contributions: R.R.F. and J.E.B conceived the idea of the analysis. M.R.B., J.H.A., and 262 J.T.M.L. conducted the modeling. C.M. processed and analyzed the GPR data. E.W.B and C.M. collected the field data. L.S.K., J.P., and S.P.G. assisted with airborne radar data processing and 263 264 identification of melt features. C.L., S.P.G., and C.L. developed the airborne radar and assisted in 265 its interpretation. J.R.M. dated and analyzed the firn cores. R.R.F. analyzed the airborne radar. 266 R.R.F., J.E.B, and M.R.B wrote the manuscript. All authors commented on the data and the 267 manuscript. 268 269 **Author Information** Reprints and permissions information is available at 270 www.nature.com/reprints. The authors declare no competing financial interests. Readers are 271 welcome to comment on the online version of the paper. Correspondence and requests for 272 materials should be addressed to R.R.F. (rick.forster@geog.utah.edu). 273

274

275

276

277

278

279

280

281

282

283

284

285

286

287

288

289

290

291

292

293

294

295

296

Fig. 1. Perennial Firn Aquifer locations on the Greenland ice sheet detected by radar and firn cores in April 2011. NASA's Operation IceBridge airborne Accumulation Radar flight lines are gray and locations of detected PFA are magenta dots. The red line represents the Arctic Circle Traverse 2011 with PFA firn-core locations and names (blue diamonds) and dry firn core locations red diamonds). The green line corresponds to the Arctic Circle Traverse 2010 that found no PFA evidences from firn cores (green diamonds). The ice sheet margin is blue and the black segment on ACT-11 line (inset) matches the GPR echogram (Fig. 2). Fig. 2. Profile of the top of the PFA from ground penetrating radar along ACT-11 traverse including PFA firn-core locations (ACT11-A and ACT11-A2). a, Surface elevation profile from simultaneously acquired GPS and topographically corrected GPR PFA top horizon. This indicates the depth to top of the firn aquifer is influenced by the local topographic slope. **b**, GPR echogram with the top of the firn aquifer as the bright contiguous horizon cutting the numerous internal firn reflecting horizons. Location of the GPR profile is shown in Fig. 1. Fig. 3. Annual snow accumulation (1958-2008) from regional climate model with output calibrated by ice core values<sup>10</sup> (color). Terrain elevation<sup>23</sup> contours are white. NASA Operation IceBridge flight lines are gray. The ACT-11 traverse is red. Locations of radar-retrieved firm aquifer positions from the OIB Accumulation Radar are illustrated as black dots. Fig. 4. Modeled liquid water content (LWC) in the firn and detected PFA from airborne radar. The simulation of LWC is from RACMO2/GR for April 2011 (color). OIB flight lines (gray), ACT-11 traverse (red) and locations of PFA from OIB radar (black dots) are all data acquired in

- April 2011. The LWC is integrated for the entire firn column from the surface down to
- approximately 20 m, varying with location (see methods for details).

Figure 1:

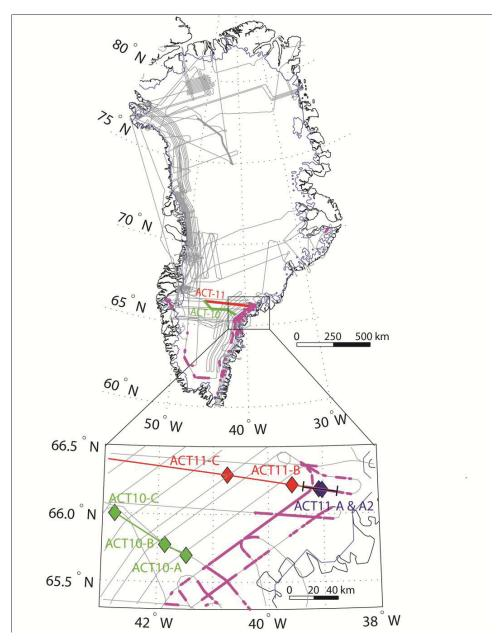


Figure 2:

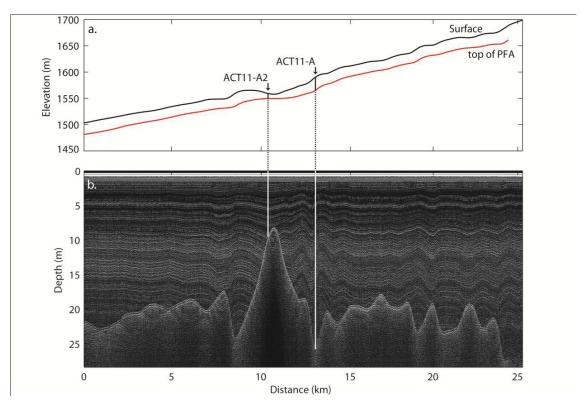


Figure 3:

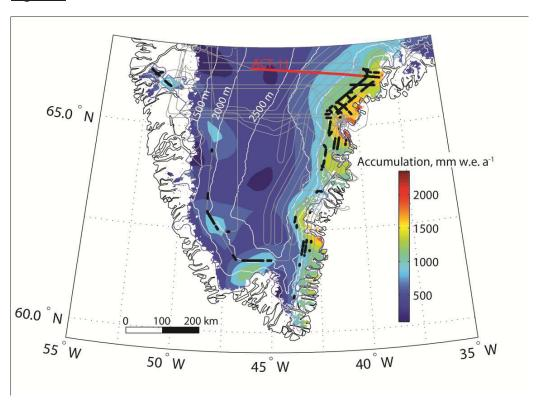


Figure 4:

